Statistical Principles of Time Reversal

K. J. Ray Liu and Beibei Wang
Origin Research
Email: {ray.liu, beibei.wang}@originwirelessai.com

***Abstract*—Time reversal is a physical principle well-known for its deterministic focusing effect. The recently discovered statistical effects shows the time-reversal focusing spot is not a point but with a Bessel power distribution. This finding offers accurate and reliable speed estimation indoors, where multipaths are abundant with mostly non-line-of-sight conditions, and enable various indoor applications such as wireless sensing and tracking. No known techniques can strive in such scenarios. In essence, time reversal is an effective tool that embraces multipaths as virtual sensors with hundreds of thousands of degrees of freedom for our utilization.**

I. Introduction

Time reversal physical principle has been known for a long time but it has largely been limited to fundamental scientific exploration [1] or niche defense applications, particularly in the field of underwater acoustic communications [2]. It has rarely been known to the general public due to its limited impact to daily life. Only until early 2000's, with the broadening of commercial radio-frequency (RF) bandwidth resulting in more resolvable multipaths, does the utilization of time reversal for extensive consumer applications using RF become possible [3].

With the ubiquity of RF radios in modern times, multipaths are abundant, and time reversal embraces multipaths, in contrast to most existing techniques that often treat multipaths as nuisances to be eliminated. Essentially, each multipath may contain valuable and distinct information along its pathway, rendering each multipath signal akin to a virtual sensor [4]. Consequently, one can imagine that the multitude of multipaths encompassing our surroundings can serve as virtual sensors that can be harnessed at will, offering new degrees of freedom for our utilization, which may not have been previously realized [5] [4].

The principle of time reversal in physics states that when a sufficient number of multipath signals are captured and time-reversed, they coalesce into a singular focal spot on a wavelength scale, resulting in a concentration of power derived from each individual multipath. In particular, when Receiver A emits a radio impulse in a multipath environment, Transmitter B receives a profile of multipaths. If Transmitter B time-reverses the profile, reversing the order of arrival such that the last goes first and the first does last, then all the multipath signals will converge at Receiver A constructively with coherent phase, resulting in the accumulation of energy at the precise focal spot [1]. As we will see in the sequel, this is just the beginning of what time reversal can offer.

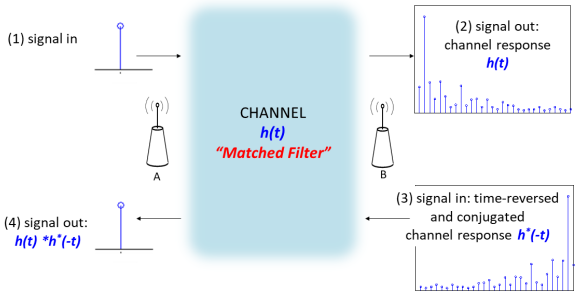

Fig. 1. Principle of Time Reversal.

II. From Physics to System Theory

From a systems theory perspective, as depicted in Fig. 1, the time-reversal effect can be understood as a flawless deconvolution process, where the surrounding space functions as an analog "computer" with infinite precision, compensating for each multipath signal received by Transceiver B and reverting it back to an impulse at Transceiver A. The presence of hundreds of thousands of multipaths is not uncommon. Achieving such a flawless deconvolution process is unattainable in digital implementations due to limitations in computing power and precision. It is worth noting that in wireless communications, typically only the 5-10 major multipaths are retained for channel equalization [6].

The perfect deconvolution results in the equalization of the channel to a distortion-free impulse response. This implies that, during time-reversal operations between the two parties, the surrounding walls and obstacles appear to have vanished. It is akin to the scenario where the two parties are communicating in the outer space without any surrounding objects, as if nothing stands between them.

It can be inferred that multipaths carry valuable indoor structural information and can be exploited to overcome obstacles. Considering that each multipath contains unique information in its own pathway, an alternative perspective is that the focusing spot is the location where information is aggregated from all the multipaths. Since each and every multipath contains certain information in their own pathway, another way to see the focusing spot is that it is where all the information, besides power, was aggregated from all the multipaths.

III. Breaking the Curse of Meter Accuracy

Let $h(k;\vec{T} \rightarrow \vec{R}_0)$ denote the k-th tap of the channel impulse response (CIR) from $\vec{T}$ to $\vec{R}_0$, where $\vec{T}$ and $\vec{R}_0$ denotes the coordinates of the transmitter (TX) and receiver (RX), respectively. In time-reversal transmission, the RX at $\vec{R}_0$ first transmits an impulse and the TX at $\vec{T}$ captures the CIR from $\vec{R}_0$ to $\vec{T}$. The TX then transmits back the time-reversed and conjugated version of the captured CIR, i.e., $h^*(-k;\vec{R}_0 \rightarrow \vec{T})$, where $*$ denotes complex conjugation. With channel reciprocity, meaning the forward and backward channels are identical, the received signal at any location $\vec{R}$ when the time-reversal waveform $h^*(-k;\vec{R}_0 \rightarrow \vec{T})$ is transmitted can be written as

$$s(k;\vec{R}) = \sum_{l=0}^{L-1} h(l;\vec{T} \rightarrow \vec{R}) h^*(l-k;\vec{R}_0 \rightarrow \vec{T}), \quad (1)$$

where L denotes the number of resolved multipaths. When $\vec{R} = \vec{R}_0$ and $k = 0$, we have $s(0;\vec{R}) = \sum_{l=0}^{L-1} |h(l,\vec{T} \rightarrow \vec{R}_0)|^2$ with all multipath components (MPCs) added up coherently, i.e., the signal energy is refocused at a particular spatial location at a specific time instance. This phenomenon is known as the time-reversal focusing effect.

In order to determine if it corresponds to the precise focusing spot, the Time-Reversal Resonating Strength (TRRS) [7] between the CIRs of two locations $\vec{R}_0$ and $\vec{R}$ can be defined as the normalized energy of the received signal when the time-reversal waveform for location $\vec{R}_0$ is transmitted:

$$\eta(\mathbf{h}(\vec{R}_0), \mathbf{h}(\vec{R})) = \frac{s(0;\vec{R})}{\sqrt{\sum_{l_1=0}^{L-1} |h(l_1;\vec{T} \rightarrow \vec{R}_0)|^2} \sqrt{\sum_{l_2=0}^{L-1} |h(l_2;\vec{T} \rightarrow \vec{R})|^2}}, \quad (2)$$

where we use $\mathbf{h}(\vec{R})$ as an abbreviation of $h(l;\vec{T} \rightarrow \vec{R})$, $l = 0, ..., L-1$, when $\vec{T}$ is fixed.

This allows for determining the exact match by utilizing the CIR or its Fourier transform, commonly referred to as the channel state information (CSI) in Wi-Fi settings, thereby enabling precise location determination without directly measuring the physical power on devices. In subsequent discussions, CSI will be used to refer to the multipath profile.

With a sufficiently large bandwidth, or equivalently, when the number of multipaths is significantly large in an indoor environment, each location will have a unique multipath profile signature [8], which can be utilized for indoor positioning purposes. Time-reversal focusing can achieve accuracy of 1-2 centimeters using a single transmitter and receiver, even in a non-line-of-sight (NLOS) environment at the 5.4 GHz Wi-Fi ISM band. This is because time-reversal focusing utilizes hundreds or even thousands of degrees of freedom (multipaths), resulting in significantly improved location accuracy, even in complete NLOS environments.

It was already well established that time of flight, signal strength, and triangulation methods could be used in wireless networks to locate a device. However, these location techniques generally require multiple sources and the accuracy is typically limited to meters, where the curse of meter accuracy was a result of having only three degrees of freedom from triangulation, and the technique only works under line-of-sight (LOS) conditions [9].

In contrast, time-reversal focusing leverages hundreds or even thousands of degrees of freedom (multipaths) resulting in much higher location accuracy while functioning in a complete NLOS environment – the more multipaths the better, contrary to the prior scientific beliefs and approaches! It can achieve accuracy at the millimeter level when using higher frequency ranges [9].

IV. A Hint to Wireless Sensing

As discussed above, different locations have their unique multipath profile signatures. In a similar way, a change in the environment, such as a door closing or opening, can significantly impact the multipath profiles and result in a shift in the time-reversal focusing point to a different location. If both locations can be accurately determined using TRRS, it enables the detection of an event, such as a door opening or closing. This phenomenon also enables the determination of changes in the environment or monitoring events using CSIs. Additionally, it can be utilized to differentiate radio-based human biometrics.

However, such a fingerprinting approach mentioned above has a drawback - it requires training to determine events by matching CSIs. If the environment is changing, even slowly, it may require frequent retraining, which limits the practical applications of these schemes.

It is logical to ask whether training can be avoided. The statistical principles of the time-reversal focusing effect discussed in the sequel offer the answer.

V. Towards Indoor Speed Estimation

Speed estimation is a crucial tool with wide-ranging applications. Outdoor environments provide ample LOS conditions for radar, telescopes, and satellites to directly observe or explore using the Doppler Effect. However, there is currently no simple and reliable/accurate method for indoor speed estimation under NLOS conditions. We will see that when a large number of multipaths are present, the time-reversal focusing spot exhibits a stationary behavior in its power distribution, following a Bessel function distribution [7]. Such a property can be used for speed estimation indoors.

Assume that all the electromagnetic (EM) waves propagate in a far-field zone, and each MPC is approximated by a plane EM wave. As illustrated in Fig. 2, the receive antenna is assumed to locate in the origin and each MPC is denoted by a point A. The coordinates of each MPC are determined by its angle of arrival θ and total traveled distance r, and $G(\omega)$ denotes the power gain with $\omega = (r, \theta)$. In a rich-scattering environment, ω can be assumed uniformly distributed in space and the total number of MPCs is large and the received signal is a scalar sum of the electric field of the impinging EM waves.

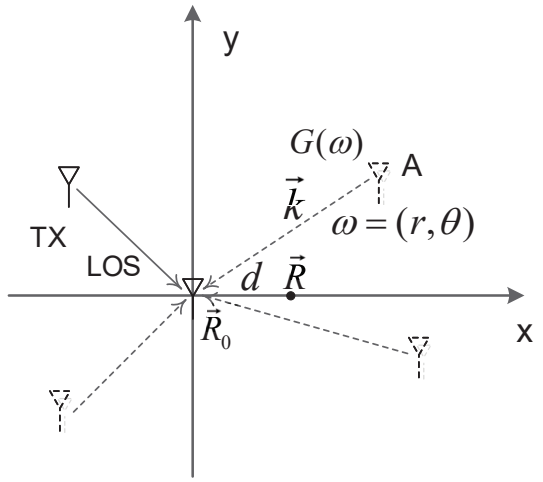

Fig. 2. Illustration of MPCs in polar coordinates [7], with the receive antenna located in the origin and each MPC denoted by a point A. The coordinates of each MPC are determined by its angle of arrival θ and total traveled distance r, and $G(\omega)$ denotes the power gain with $\omega = (r, \theta)$.

For any point $\vec{R}$ in a source-free region with constant mean electric and magnetic fields, the channel impulse response when a rectangular pulse is transmitted can be written as

$$h(t; \vec{T} \to \vec{R}) = \sum_{\omega \in \Omega} G(\omega) e^{j(2\pi f_0 (t - \tau(\omega)) - \phi(\omega) - \vec{k}(\omega) \cdot \vec{R})}, \quad (3)$$

where $\tau(\omega) = r/c$ is the propagation delay of the MPC ω, f_0 is the carrier frequency, Ω is the set of MPCs, $\phi(\omega)$ is the change of phase due to reflections, $\vec{k}(\omega)$ is the wave vector with amplitude $k = c/f_0$, and c is the speed of light. Accordingly, the l-th tap of a sampled CIR at location $\vec{R}$ can be expressed as

$$h(l; \vec{T} \to \vec{R}) = \sum_{\tau(\omega) \in [lT - \frac{T}{2}, lT + \frac{T}{2})} G(\omega) e^{j(2\pi f_0 \Delta\tau(l,\omega) - \phi(\omega) - \vec{k}(\omega) \cdot \vec{R})} \quad (4)$$

where T is the channel measurement interval and $\Delta\tau(l, \omega) = lT - \tau(\omega)$ for $l = 0, 1, ..., L-1$.

The received signal at each point $\vec{R}$ when the time-reversal waveform $h^*(-l; \vec{R}_0 \to \vec{T})$ is transmitted can be approximated from (1) as

$$s(0; \vec{R}) \approx \sum_{l=1}^{L} |G(m)|^2 e^{-j\vec{k}(m) \cdot (\vec{R} - \vec{R}_0)}. \quad (5)$$

When the bandwidth is sufficiently large, without loss of generality, with multipaths arriving from all directions such that the power distribution of MPC is uniform in direction θ, meaning $G(\omega)$ only depends on r and approximately the same for any θ [7], the received signal $s(0; \vec{R})$ can further be approximated as

$$\begin{aligned} s(0; \vec{R}) &= \sum_{\omega \in \Omega} |G(\omega)|^2 e^{-j\vec{k} \cdot (\vec{R} - \vec{R}_0)} \\ &\approx \int_0^{2\pi} P(\theta) e^{-jkd\cos(\theta)} d\theta \\ &= P J_0(kd), \end{aligned} \quad (6)$$

where the discrete sum is approximated by a continuous integral, Ω stands for the set of all significant MPCs, $J_0(x)$ is the 0^{th}-order Bessel function of the first kind $J_0(x) = \frac{1}{2\pi} \int_0^{2\pi} \exp(-jx\cos(\theta)) d\theta$, and d is the Euclidean distance between $\vec{R}_0$ and $\vec{R}$. What (6) says is that the power distribution at the time-reversal focusing spot is of Bessel function distribution.

As practical power measurement is not feasible, we can resort to the TRRS, which is a type of cross-correlation that allows us to measure this effect via CSIs. For $\vec{R} = \vec{R}_0$, it degenerates to the case of $d = 0$ and thus $s(0; \vec{R}_0) \approx P$, which is the peak of the focusing spot. As a result, the TRRS defined in (2) can is given by [7]

$$\eta(\mathbf{h}(\vec{R}_0), \mathbf{h}(\vec{R})) = J_0(kd). \quad (7)$$

Essentially, the requirement is for an RF device to possess a sufficiently large bandwidth to capture a substantial number of multipaths, regardless of the surrounding geometry. Remarkably, the time-reversal focusing spot is not a point, but rather possesses a structure that is independent of location and environment. This property renders it ideal for indoor speed estimation.

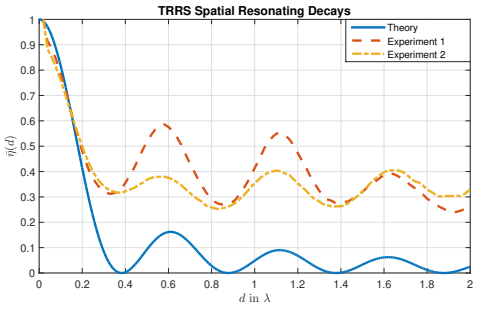

Fig. 3. Comparison of the TRRS distribution between experimental results and the theoretical result [7], where the carrier frequency of the transmitted signal is at 5.8 GHz with $\lambda = 5.17$ cm.

Fig. 3 illustrates two experimental results obtained at Location 1 and Location 2, which are 10m apart. The distance d from each predefined focal spot is varied from 0 to 2λ. The measured TRRS distribution functions exhibit good agreement with the theoretical prediction. Specifically, the positions of the peaks and valleys in the measured curves match to those of the theoretical curve. Since the TRRS distribution function depends only on the distance between two points, without abuse of terminology, we can simply use $\eta(d) = J_0(kd)$ to represent the TRRS approximation between two points separated by

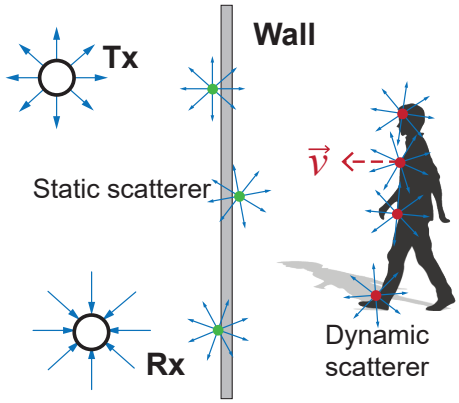

Fig. 4. Multipath model for rich-scattering indoor environments, where objects scatter the signal and produce many paths [10].

a distance d. The shape of the TRRS distribution function $\eta(d) = J_0(kd)$ is determined solely by the wave number k which is independent of specific locations. Therefore, the TRRS distribution function can be used as an intrinsic ruler to measure distances in space.

For instance, consider an RX moving along a straight line at a constant speed v starting from location $\vec{R}_0$, and a TX keeps transmitting the time-reversal waveforms corresponding to $\vec{R}_0$ at regular intervals. The TRRS measured at the RX is a sampled version of $\eta(d)$ and exhibit the Bessel-function-like pattern. We can estimate the speed of the RX by measuring the time $\hat{t}$ it takes for the RX to reach the first local peak starting from $\vec{R}_0$. The speed can be estimated as $\hat{v} = (0.61\lambda)/\hat{t}$, where $d \approx 0.61\lambda$ is the theoretical distance corresponding to the first local peak of the Bessel-function-like pattern [7].

Many existing techniques, including the Doppler Effect, experience performance degradation in the presence of multipaths, even under LOS conditions. Finally, the speed and distance can now be accurately and reliably estimated in indoor environments. Contrary to prior scientific approaches, the performance improves with an increase in the number of multipaths.

An immediate application that can be observed is indoor tracking. IoT devices can utilize CSIs from ambient radios to calculate their own speed. By utilizing an inertial measurement unit, which is commonly available in smartphones or IoT devices for directional information, in conjunction with a geolocation map, an unlimited number of users can be tracked [7].

VI. Virtual Time-Reversal Effect

As discussed above, speed estimation with one device (e.g., RX) moving is feasible. However, in cases where there is no active source to generate a physical time-reversal effect, what can be done? Fig. 4 illustrates that when an object moves in a space filled with ambient radio waves, it appears as if there are multiple dynamic scatterers on the object, moving at the same velocity. Each dynamic scatterer can be considered as a virtual passive source with low radiation power. Therefore, resorting to collective statistics is necessary to uncover their common collective behavior.

According to the superposition principle of EM waves, the CSI $H(t,f)$ can be decomposed as

$$H(t,f) = \sum_{i\in\Omega_s(t)} H_i(t,f) + \sum_{j\in\Omega_d(t)} H_j(t,f) + \varepsilon(t,f), \quad (8)$$

where $\Omega_s(t)$ represents the set of static scatterers, $\Omega_d(t)$ represents the set of dynamic scatterers, and $H_i(t,f)$ denotes the part contributed by the i-th scatterer. The noise term $\varepsilon(t,f)$ is the additive white Gaussian noise with variance $\sigma^2(f)$ and is statistically independent of $H_i(t,f)$ [11]. The decomposition is based on the fact that each scatterer acts as a "virtual transmitter" scattering the EM waves in all directions, and the received EM waves add up at the receive antenna from the reflecting off the interior objects in indoor environments. Consequently, $H(t,f)$ measures the sum of the electric fields of all the incoming EM waves. In practice, assuming that both the sets $\Omega_s(t)$ and $\Omega_d(t)$ change slowly over a sufficiently short period of time, they can be approximated as time-invariant sets.

Without loss of generality, let us consider a 2-D scattering model where all the scatterers are within the same horizontal plane. Due to channel reciprocity, EM waves traveling in both directions undergo the same physical perturbations, such as reflection, refraction, diffraction. Thus, if the receiver transmits EM waves, the CSI "measured" at the i-th scatterer or "virtual transmitter" would be identical to $H_i(t,f)$. As $H_i(t,f)$ actually measures the electric fields, $\vec{E}_i(t,f) = \int_0^{2\pi} \vec{F}(\theta,f)\exp(-j\vec{k}\cdot\vec{v}_i t)\mathrm{d}\theta$, of the incoming EM waves, where the speed of the i-th scatterer is v_i, $H_i(t,f)$ can be expressed as

$$H_i(t,f) = \int_0^{2\pi} F_i(\theta,f)\exp\left(-jkv_i\cos(\theta)t\right)d\theta, \quad (9)$$

where $F_i(\theta,f)$ denotes the complex channel gain of the MPC from the direction θ for the i-th scatterer, and k is the wave number.

Note that the mean of $H_i(t,f)$ is zero, which is represented as $\mathbb{E}[H_i(t,f)] = 0$, where $\mathbb{E}[\cdot]$ denotes the expectation operator. The covariance of two CSI values with time lag τ can be expressed as [11]

$$\begin{aligned}\mathrm{Cov}\left[H_i(t,f), H_i(t+\tau,f)\right] &= \mathbb{E}\left[H_i(t,f)H_i^*(t+\tau,f)\right] \\ &\approx 2\pi\sigma_{F_i}^2(f)J_0(kv_i\tau), \quad (10)\end{aligned}$$

where $J_0(\cdot)$ is the 0^{th}-order Bessel function of the first kind, $\sigma_{F_i}^2(f)$ is the variance of $F_i(\theta,f)$, and $F_i(\theta,f)$ is assumed to be a circular-symmetric Gaussian random variable with the same variance for $\forall\theta$. The ACF of $H_i(t,f)$ with time lag τ, denoted as $\rho_{H_i}(\tau,f)$, is derived as

$$\begin{aligned}\rho_{H_i}(\tau,f) &= \frac{\mathrm{Cov}\left[H_i(t,f), H_i(t+\tau,f)\right]}{\mathrm{Cov}\left[H_i(t,f), H_i(t,f)\right]} \\ &= J_0(kv_i\tau). \quad (11)\end{aligned}$$

Consider that only one object is moving, and the speeds of all the scatters caused by the object are approximated to

be the same $v_i = v$, for $\forall i \in \Omega_d$. Then, the autocorrelation function (ACF) of the CSI $H(t, f)$ with time lag τ, denoted as $\rho_H(\tau, f)$, can be obtained as

$$\rho_H(\tau, f) = \alpha(f) J_0(kv\tau), \tag{12}$$

where $\alpha(f)$ is the gain of each subcarrier f. When all frequencies are considered, the $\alpha(f)$ factor will be aggregated and disappear. Equation (12) is equivalent to (7), where the only difference is that (7) is viewed from the power distribution perspective with $d = v\tau$.

VII. Reflection

It is not surprising that the ACF also follows the Bessel function, as it is also a second-order statistics like TRRS and shares the same mathematical expression. In essence, a moving object can be regarded as a collection of virtual sources, and their combined strength can be revealed through statistical electromagnetics, as a result of a virtual time-reversal focusing effect [9] [11]!

Now the active and passive sources are integrated into a unified time-reversal framework in that we can state that the second order statistics, either TRRS of active sources or ACF of passive sources, exhibits Bessel function distributions owing to the time-reversal Bessel power distribution at the focusing spot. We can simply write

$$\rho(\tau) = J_0(kv\tau), \tag{13}$$

where $\rho(\cdot)$ stands for the second-order statistics of time-reversal effects, τ is the time lag, $k = c/f$ is the wave number, and v is the speed, which can be estimated accurately and reliably under multipath conditions, even for indoor NLOS conditions.

If one relooks at (6), he/she will find that this equation is satisfied when there are many multipaths uniformly arriving from every direction, which is the case for multipath-rich indoor scenarios. It implies the received power distribution at the receiver should also follow the Bessel distribution, even when there is no time reversal operation. It has been observed long ago by Clarke [12] that the spatial autocovariance function of the electric field under multipath-rich environment is a Bessel function. But he fell short of concluding this phenomenon was due to the power distribution is of Bessel function. A reason was because no one looks at it at one particular time instance like the moment of time reversal focusing to see the effect. In communications, signals keep coming in so that every Bessel power distribution is collated and aggregated resulting in seeing only the power envelope, i.e., the effect of each individual Bessel function disappears. Time reversal allows us to see a particular instant when all the multipaths all come together to clearly exhibit the Bessel effect. But at every instant, there are still all the multipaths coming and mixing together, albeit not completely in phase like time reversal, and the power distribution is still Bessel. That helps explain why the spatial correlation under multipath conditions as observed by Clarke is Bessel.

VIII. Enabling Reliable Wireless Sensing

The relation $\rho(\tau) = J_0(kv\tau)$ can be evaluated with CSIs, which are readily available in the ambient radio waves of ubiquitous Wi-Fi and 5G/6G systems [13]. Falls have been a significant concern in elder care due to their potential for severe consequences. Falls are characterized by a distinctive motion, wherein the body continues to accelerate and then experiences a sudden, forceful deceleration, setting them apart from other typical human motions (see Fig. 5). This distinctive feature can be exploited for accurate fall detection, provided that the speed can be accurately measured [11].

Despite being bipedal, each individual walks in a distinct manner. Gait patterns (see Fig. 6), including stride length and walking cadence, can be deduced from speed information [10]. Human motions can also be inferred from the motions of pets or machines (e.g. iRobot, fan, etc.). Motion statistics can be used to sensitively detect slight human motions for presence or intrusion detection, and for automatic control of lightbulbs, TVs, air conditioners for energy management. Breathing can also be easily monitored for sleep monitoring, all without the need for wearables.

Millimeter wave radio can be utilized to pick up heartbeats for inferring heart rate variability, sound for enhancement or separation, and other applications such as gesture, handwriting, and keystroke recognition, all using only commodity Wi-Fi without the need for wearables.

IX. Relation to Massive MIMO

We have seen a powerful/universal time reversal-based statistical tool for speed estimation by treating the massive multipaths (indoors) as virtual sensors. Is it possible to compare the utilization of hundreds of thousands of virtual sensors with a large number of real antennas in massive MIMO as commonly used in 5G/6G communications? To characterize the power distribution of the focusing effect and investigate its relationship with a target's motion, similar to the above, we can define the ACF of the received signal in massive MIMO similarly.

Assume a receiver is located on a mobile object/target and receives a signal transmitted from a base station (BS) with M antennas, where $\mathbf{r}_t$ denotes the receiver's location at time t. A_e denotes the aperture of the antenna. The received signal comprises both LOS and NLOS components and can be expressed as follows [14]:

$$\begin{aligned} y(t) &= y_{\mathrm{L}}(t) + y_{\mathrm{N}}(t) + n(t), \\ y_{\mathrm{L}}(t) &= \sqrt{K_{\mathrm{L}}} \sum_{m=1}^{M} \frac{\exp(j(k|\mathbf{x}_m \mathbf{r}_t| + \phi_m))}{4\pi |\mathbf{x}_m \mathbf{r}_t|}, \\ y_{\mathrm{N}}(t) &= \sqrt{K_{\mathrm{N}}} \sum_{n=1}^{N} \exp[j(\omega_d t \cos\alpha_n + \phi_n)], \end{aligned} \tag{14}$$

where $y_{\mathrm{L}}(t)$ and $y_{\mathrm{N}}(t)$ represent LOS and NLOS component with power coefficient K_{L} and K_{N}, and N is the total number of NLOS signal components. k denotes the wave number. ω_d is the maximum Doppler frequency. $\mathbf{x}_m$ and $\mathbf{r}_t$ are the coordinates of the m-th antenna and the receiver at time t,

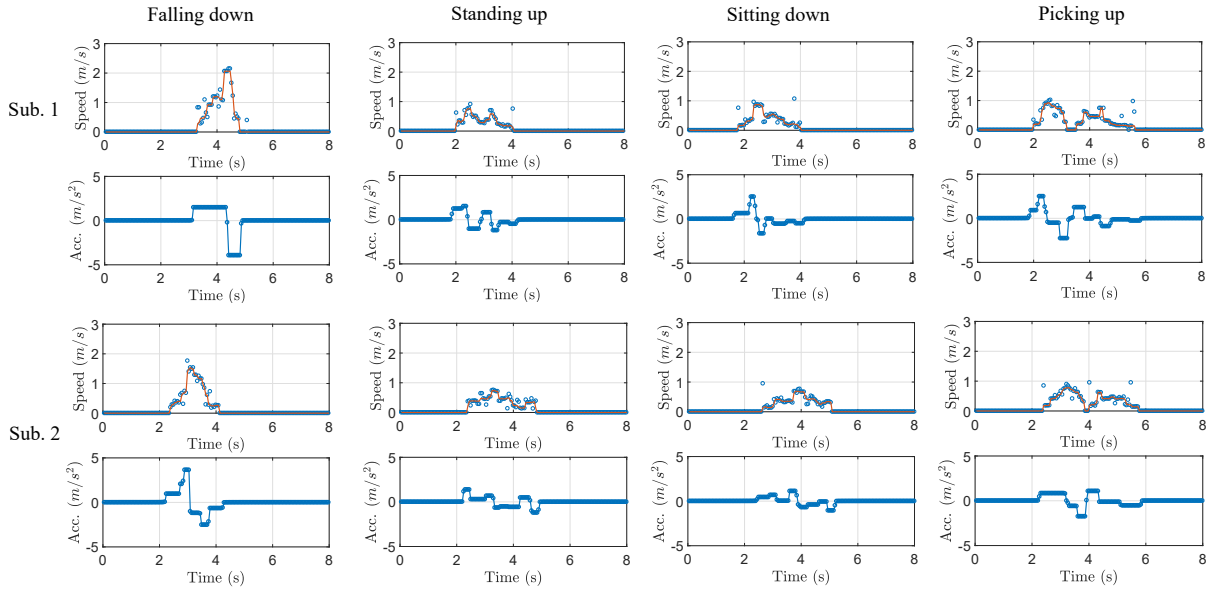

Fig. 5. Speed and acceleration (Acc.) for different activities and subjects (Sub. 1 and Sub. 2) [11].

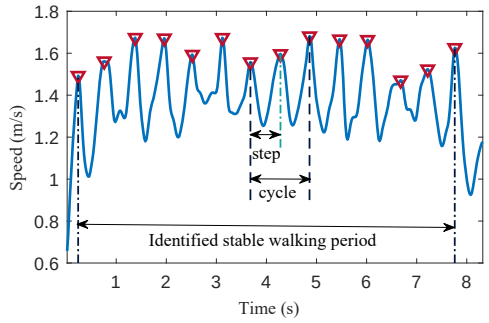

Fig. 6. Illustration of gait cycle, defined as the duration between two consecutive events that the same heel hits the ground during walking. During normal human walking, a subject's speed experiences an increase then a decrease, resulting in a speed peak for each step [10]. The carrier frequency is at 5.8 GHz with a bandwidth of 40 MHz and a sampling rate 1500 Hz.

respectively, $|\mathbf{x}_m\mathbf{r}_t|$ denotes the distance between $\mathbf{x}_m$ and $\mathbf{r}_t$. $n(t)$ is the additive Gaussian noise while ϕ_m is the phase distortion of the m-th LOS signal. α_n and ϕ_n are the DOA and phase distortion of the n-th NLOS signal component. In general, ϕ_m, α_n, and ϕ_n can be assumed as i.i.d uniformly distributed over $[-\pi, \pi)$.

Based on (14), the ACF of the received signal can be expressed as

$$\eta_y(\mathbf{r}_0, \mathbf{r}_s) = \mathbb{E}[y(t_0)y^*(t_s)] \approx \eta_{y_{\text{L}}} + \eta_{y_{\text{N}}} + \eta_{\text{n}}, \tag{15}$$

where $\eta_{y_{\text{N}}} = K_{\text{N}}NJ_0(kd)$ is similar to the derivation in Section V. $\mathbb{E}$ represents expectation operator and $J_0(\cdot)$ is the 0-order Bessel function while d denotes the distance between $\mathbf{r}_0$ and $\mathbf{r}_s$. The ACF of the LOS signal can be given by [14]

$$\eta_{y_{\text{L}}} = \frac{\text{A}_e \exp(jk\boldsymbol{\epsilon})}{z} \text{sinc}(\frac{k\boldsymbol{\xi}\text{A}_e}{2L}), \tag{16}$$

where $\boldsymbol{\epsilon}$ and $\boldsymbol{\xi}$ represent the range and cross-range between $\mathbf{r}_0$ and $\mathbf{r}_s$, z represents the inner element space in the transmit antenna array, $\text{sinc}(t) = \sin(t)/t$ is the sinc function, under the far-field condition. Then, the ACF of the received signal can be expressed as

$$\eta_y(\mathbf{r}_0, \mathbf{r}_s) = \frac{\text{A}_e \exp(jk\boldsymbol{\epsilon})}{z} \text{sinc}(\frac{k\boldsymbol{\xi}\text{A}_e}{2L}) + K_{\text{N}}NJ_0(kd) + \sigma^2\mathbf{I}, \tag{17}$$

where σ^2 is the power spectral density of the noise $\text{n}(t)$.

It has been shown in [14] that $K_{\text{N}}NJ_0(kd)$ decays much faster than $\text{sinc}(\frac{k\boldsymbol{\xi}\text{A}_e}{2L})$. Therefor the LOS component dominates the effect and the $J_0(kd)$ term can be ignored. When there is no LOS component, it degenerates to the same time-reversal effect discussed in prior sections. In either case, the speed estimation can be done similarly as well.

X. Conclusions

Most existing techniques rely on LOS observations and attempt to minimize the effects of multipath propagation. In contrast, time reversal embraces and strives on multipaths, the more the better, contrary to most existing paradigms. It offers accurate and reliable speed estimation and uncovers new thinking and solutions ideal for indoor applications, especially under NLOS conditions, long considered difficult and challenging due to multipath effects.

Peter Siegel stated in [9] that the statistical effects of time-reversal that can be described by the simple yet beautiful equation $\rho(\tau) = J_0(kv\tau)$ *"represents a unique solution to the almost two-century long quest for some new physics that could equal, and in this case surpass, the ubiquitous frequency vs. speed relationship between a moving object and a wave-based source first described by Christian Doppler in 1842."* Time reversal strives with multipaths, while on the other hand,

Doppler Effect does without. Therefore, both complement each other well and offer two distinct approaches to unlock unlimited possibilities in future applications.

REFERENCES

[1] M. Fink, "Time reversal of ultrasonic fields: Part i—basic principles," *IEEE Transactions on Ultrasonics, Ferroelectrics and Frequency Control*, vol. 39, no. 5, pp. 555–566, 1992.

[2] W. Kuperman, W. S. Hodgkiss, H. C. Song, T. Akal, C. Ferla, and D. R. Jackson, "Phase conjugation in the ocean: Experimental demonstration of an acoustic time-reversal mirror," *Journal of the Acoustical Society of America*, vol. 103, no. 1, pp. 25–40, 1998.

[3] B. Wang, Y. Wu, F. Han, Y.-H. Yang, and K. J. R. Liu, "Green wireless communications: A time-reversal paradigm," *IEEE Journal on Selected Areas in Communications*, vol. 29, no. 8, pp. 1698–1710, 2011.

[4] K. J. R. Liu and B. Wang, *Wireless AI: Wireless Sensing, Positioning, IoT, and Communications*. Cambridge University Press, 2019.

[5] B. Wang, Q. Xu, C. Chen, F. Zhang, and K. J. R. Liu, "The promise of radio analytics: A future paradigm of wireless positioning, tracking, and sensing," *IEEE Signal Processing Magazine*, vol. 35, no. 3, pp. 59–80, 2018.

[6] K. Cheun, "Performance of direct-sequence spread-spectrum rake receivers with random spreading sequences," *IEEE Transactions on Communications*, vol. 45, no. 9, pp. 1130–1143, 1997.

[7] F. Zhang, C. Chen, B. Wang, H.-Q. Lai, Y. Han, and K. J. R. Liu, "WiBall: A time-reversal focusing ball method for decimeter-accuracy indoor tracking," *IEEE Internet of Things Journal*, vol. 5, no. 5, pp. 4031–4041, 2018.

[8] Z.-H. Wu, Y. Han, Y. Chen, and K. J. R. Liu, "A time-reversal paradigm for indoor positioning system," *IEEE Transactions on Vehicular Technology*, vol. 64, no. 4, pp. 1331–1339, 2015.

[9] P. H. Siegel, "Ieee president k. j. ray liu, "follow multiple paths," changing the world with microwave time reversal focusing," *IEEE Journal of Microwaves*, vol. 2, no. 3, pp. 360–373, 2022.

[10] C. Wu, F. Zhang, Y. Hu, and K. J. R. Liu, "GaitWay: Monitoring and recognizing gait speed through the walls," *IEEE Transactions on Mobile Computing*, vol. 20, no. 6, pp. 2186–2199, 2021.

[11] F. Zhang, C. Chen, B. Wang, and K. J. R. Liu, "WiSpeed: A statistical electromagnetic approach for device-free indoor speed estimation," *IEEE Internet of Things Journal*, vol. 5, no. 3, pp. 2163–2177, 2018.

[12] R. H. Clarke, "A statistical theory of mobile-radio reception," *The Bell System Technical Journal*, vol. 47, no. 6, pp. 957–1000, 1968.

[13] C. Wu, B. Wang, O. C. Au, and K. J. R. Liu, "Wi-fi can do more: Towards ubiquitous wireless sensing," *IEEE Communications Standards Magazine*, vol. 6, no. 2, pp. 42–49, June 2022.

[14] X. Zeng, F. Zhang, B. Wang, and K. J. R. Liu, "Massive mimo for high-accuracy target localization and tracking," *IEEE Internet of Things Journal*, vol. 8, no. 12, pp. 10 131–10 145, 2021.